Autonomous T cell trafficking examined *in vivo* with intravital two-photon microscopy

Mark J. Miller*, Sindy H. Wei*, Michael D. Cahalan*†‡, and Ian Parker†§

Departments of *Physiology and Biophysics and §Neurobiology and Behavior, University of California, Irvine, CA 92697

Communicated by Mark M. Davis, Stanford University School of Medicine, Stanford, CA, December 31, 2002 (received for review October 22, 2002)

The recirculation of T cells between the blood and secondary lymphoid organs requires that T cells are motile and sensitive to tissue-specific signals. T cell motility has been studied *in vitro*, but the migratory behavior of individual T cells *in vivo* has remained enigmatic. Here, using intravital two-photon laser microscopy, we imaged the locomotion and trafficking of naïve CD4$^+$ T cells in the inguinal lymph nodes of anesthetized mice. Intravital recordings deep within the lymph node showed T cells flowing rapidly in the microvasculature and captured individual homing events. Within the diffuse cortex, T cells displayed robust motility with an average velocity of $\approx$11 μm·min^{-1}. T cells cycled between states of low and high motility roughly every 2 min, achieving peak velocities >25 μm·min^{-1}. An analysis of T cell migration in 3D space revealed a default trafficking program analogous to a random walk. Our results show that naïve T cells do not migrate collectively, as they might under the direction of pervasive chemokine gradients. Instead, they appear to migrate as autonomous agents, each cell taking an independent trafficking path. Our results call into question the role of chemokine gradients for basal T cell trafficking within T cell areas and suggest that antigen detection may result from a stochastic process through which a random walk facilitates contact with antigen-presenting dendritic cells.

CD4$^+$ T cells play a pivotal role in the initiation and subsequent coordination of the immune response. Recirculation of naïve T cells between the blood and secondary lymphoid organs is critical for the detection of foreign antigens in tissues throughout the body (1–4), and the organized structure of lymphoid tissues (5, 6) makes it possible for T cells to sample a local landscape of antigen, discriminating foreign from self-determinants. Evidence has been reviewed recently (7–11) that chemokine gradients orchestrate the cellular organization of the lymphoid organs and direct the trafficking of lymphocytes within these tissues. However, these dynamic phenomena have never been observed *in vivo*. Despite the enormous progress in understanding the molecular and cellular details that shape the immune response, we still know little about the motility and migratory behavior of individual T cells as they pass through the secondary lymphoid organs (12).

Lymphocyte function is contingent on numerous environmental factors that cannot readily be replicated by *in vitro* studies. For example, motility has been studied *in vitro* by using activated T cells and T cell lines on a variety of substrates, but with little consensus on velocities or control by intracellular signaling pathways (13–17). Moreover, striking differences in T cell/antigen-presenting cell interaction dynamics and activation requirements have been observed depending on the culture system (16, 18–20). Clearly, *in vivo* studies are essential for understanding lymphocyte function as it occurs in the natural tissue environment. Intravital microscopy has been successfully used to study the homing and dynamics of T and B cells in postcapillary venules (21, 22), but these bright-field and standard fluorescence techniques do not permit the discrimination of individual cells in the cellular compartments of the lymph node. Recently, two-photon (2P) imaging (23) has allowed a tantalizing look at living lymphocytes hundreds of microns inside explanted lymphoid tissues (24, 25) and in a reconstituted thymocyte coculture system (26). Here, we introduce intravital 2P microscopy for high-resolution imaging of T cells deep within the lymphoid organs of a living mouse. This allows the motility of lymphocytes to be analyzed *in vivo* and enables trafficking theories to be assessed directly. We show that migrating T cells move autonomously, with each cell taking an independent and apparently random 3D path through the T cell areas of the lymph node. The results presented here expand our understanding of individual T cell behavior and have important implications for lymphoid tissue organization and antigen recognition.

Materials and Methods

Adoptive Transfer of CD4$^+$ Naïve T Cells. Naïve CD4$^+$ T cells bearing a monoclonal T cell receptor specific for chicken ovalbumin were isolated from DO11.10 transgenic mice by using magnetic negative selection (CD4 isolation kit, Miltenyi Biotec, Auburn, CA) and labeled with carboxyfluorescein diacetate succinimidyl ester (CFSE, Molecular Probes) as described (24). Ten million labeled T cells (>95% CD4$^+$ by flow cytometry) were adoptively transferred by tail vein injection into 4-week-old BALB/c recipient mice.

Intravital Imaging. One day after adoptive transfer, the recipient mouse was anesthetized with an i.p. injection of Avertin (tribromoethanol, Sigma) at 360 mg/kg, with repeated doses (180 mg/kg) administered as required (27). Avertin induced a plane of anesthesia sufficient to immobilize the animal without overly depressing respiration or causing other complications (28). To ensure adequate tissue oxygenation, a stream of 95% O_2/5% CO_2 was delivered to a mask that covered the snout. We developed an intravital chamber (Fig. 1) that minimized respiratory movement artifacts yet maintained tissue viability. T cells remained fully motile with no evidence of decreased viability for experiments lasting up to 4 h. The inguinal lymph node was surgically exposed on a skin flap, and a rubber O-ring (17 mm outside diameter) was glued (Vetbond, 3M Co.) on the inner membrane. The mouse was then placed on a custom-made imaging platform, with the skin flap raised on a copper heating block. A flanged Plexiglas support was carefully lowered onto the O-ring to dampen movement artifacts caused by respiration and sealed with Vaseline to form a watertight chamber filled with PBS. Both the chamber and mouse were warmed, and the temperature in the imaging chamber was maintained at 35–36°C via a thermistor placed in the saline solution. Our paramount concern in these studies was to preserve the normal physiology of the tissue and prevent potential damage to the circulatory, lymphatic, and nervous connections. Therefore, we imaged only through naturally occurring "windows" present at various locations in the overlying fat pad in 4-week-old mice. Blood vessels within the lymph node were revealed after i.v. injection of 200

Abbreviations: CFSE, carboxyfluorescein diacetate succinimidyl ester; HEV, high-endothelial venule; 2P, two-photon.

†M.D.C. and I.P. contributed equally to this work.

‡To whom correspondence should be addressed. E-mail: mcahalan@uci.edu.

www.pnas.org/cgi/doi/10.1073/pnas.2628040100

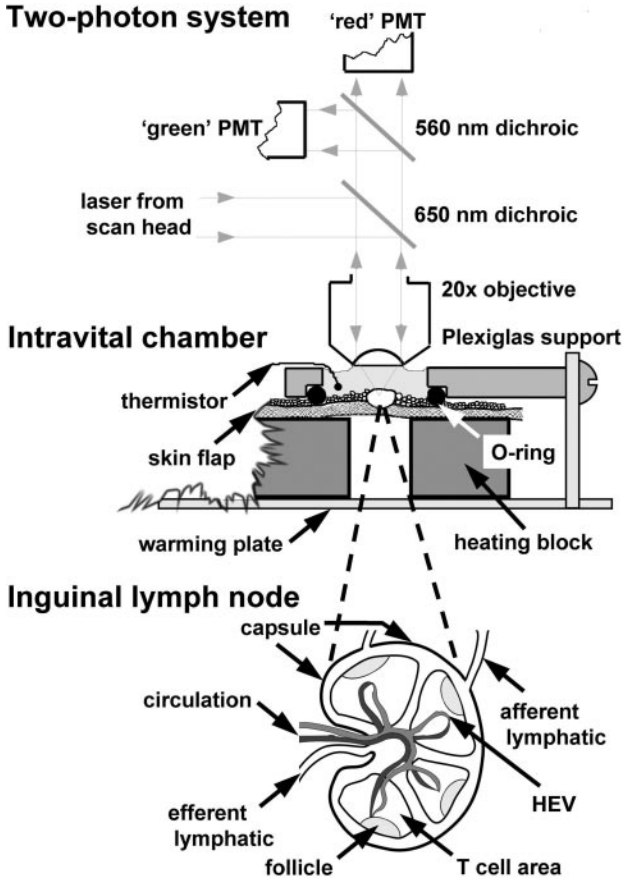

Fig. 1. Intravital 2P imaging system. (*Top* and *Middle*) Schematic diagram of the 2P microscope and intravital imaging chamber. PMT, photomultiplier tube. (*Bottom*) The structure of a lymph node, showing the relative positions of B cell follicles, T cell areas in the diffuse cortex, HEVs, overlying capsule, and lymphatic and circulatory connections.

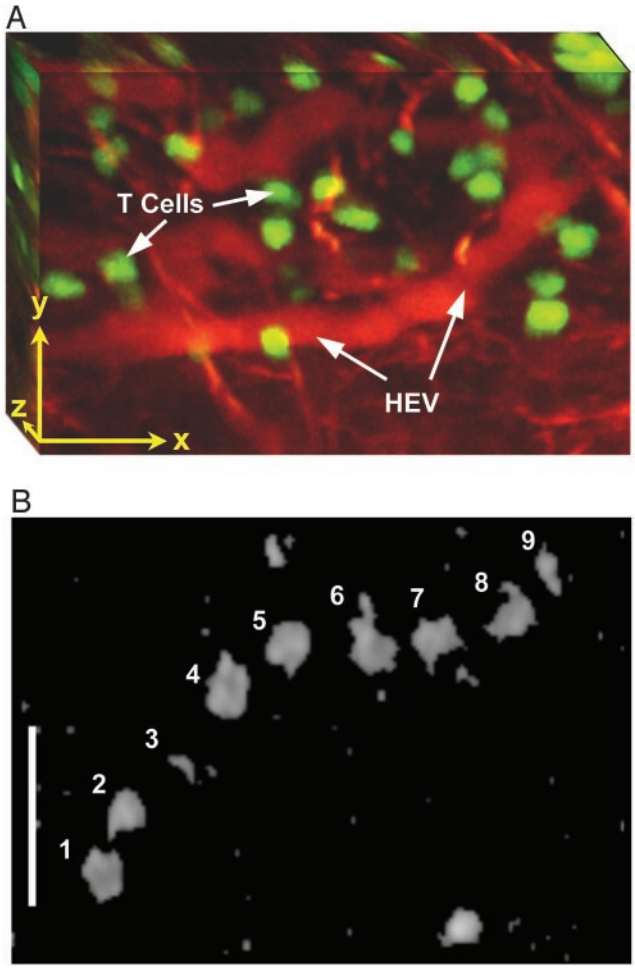

Fig. 2. Intravital imaging of vessels and cells in a living lymph node. (*A*) 3D reconstruction representing a 85 × 120 × 75-μm volume of the T cell area, centered 120 μm below the surface of the lymph node. (Scale bars, 30 μm in all axes.) CFSE-labeled naïve T cells (green) are observed in the vicinity of a presumptive HEV (red), identified by i.v. injection of tetramethylrhodamine dextran. (*B*) Video-rate imaging of a T cell flowing in a small vessel within a T cell region of the node. Image is a superposition of nine consecutive video frames acquired at 34-ms intervals and shows the progression of a single CFSE-labeled T cell traveling at ≈20 mm·min^{-1} (0.03 cm·s^{-1}) within a blood vessel. (Scale bar, 25 μm.)

μl of 10 mg/ml tetramethylrhodamine dextran (10 kDa, Molecular Probes).

2P Microscopy and Image Analysis. Imaging was performed with a custom-built system (29) as described (24), except that a second photomultiplier tube detector channel was added to permit simultaneous imaging of labeled T cells (green) and blood vessels (red) (Fig. 1). In brief, the system was based on an upright Olympus BX50 microscope fitted with a ×20 water-immersion objective (numerical aperture = 0.95), a Spectra-Physics Tsunami femtosecond laser tuned to 780 nm, a resonant-mirror scan head, and a motorized focus controller (Prior Scientific, Rockland, MA). Image acquisition operated under software control (METAMORPH, Universal Imaging, Downingtown, PA). For imaging motility, 3D image stacks (x, y, z) were acquired at a single wavelength (green) as follows: each x–y plane spanned 175 × 225 μm at a resolution of two pixels per μm^{-1} and was formed by averaging nine video frames. Seventeen sequential planes were acquired at axial (z) spacing of 3 μm to form a z-stack at each 10-s time point. Data sets were flattened along the z axis as maximum intensity projections representing a "top" (x–y) view of the volume. To track axial movements in our imaging volume, depth information was encoded by generating color images from three overlapping segments (top, middle, and bottom) of the z-stack, assigned the colors red, green, and blue, respectively. After flattening to generate a top view, this created an image sequence with a five-color spectrum (three primary colors and two overlap colors), each color representing a discrete depth range in the volume.

Results

Intravital 2P Imaging of Naïve T Cells in Lymph Nodes. Our current understanding of T cell motility and migration in lymph nodes derives from indirect evidence, because it has not been possible to observe these dynamic processes *in vivo*. To study the default migratory behavior of naïve T cells, we used CFSE-labeled CD4$^+$ T cells with monoclonal antigen specificity from TCR transgenic DO11.10 mice to avoid activation in response to environmental antigens. Cells were imaged by intravital 2P microscopy in inguinal lymph nodes 16–18 h after adoptive transfer into recipient BALB/c mice. In some experiments, blood vessels were made visible by i.v. injection of tetramethylrhodamine dextran to provide a landmark for identification of canonical T cell zones. For example, Fig. 2*A* shows a 3D reconstruction in which T cells (green) congregated ≈150 μm below the capsule near a small vessel (red) that displayed the kinked, hairpin-loop morphology characteristic of high endo-

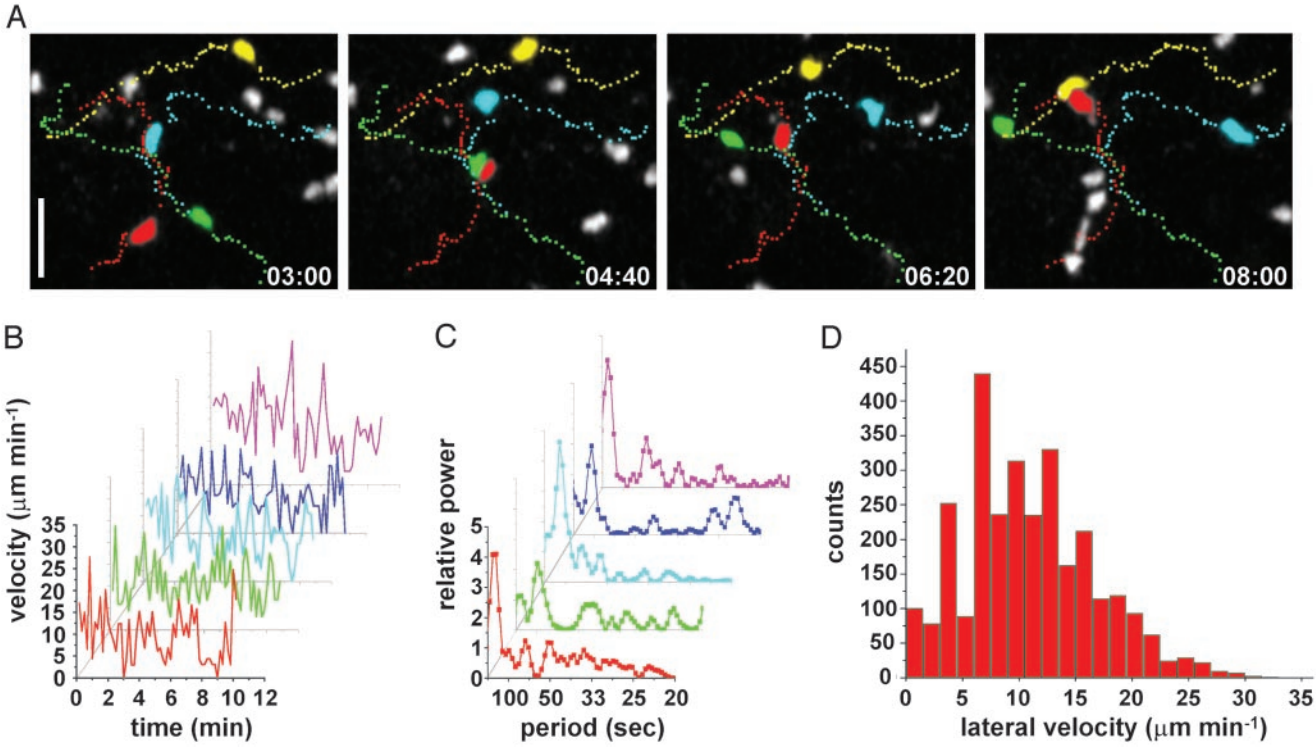

Fig. 3. *In vivo* motility of T cells. (*A*) Sequence of images at ≈1-min intervals illustrating T cell migration. Each panel shows a compression along the *z* axis (top view) derived from a 51-μm-deep *z*-stack. Four individual cells and their corresponding tracks (dots tracked at intervals of 10 s) are pseudocolored for illustration. Times are in min/s. (Scale bar, 20 μm.) (*B*) Velocity fluctuations of five individual T cells. Velocities were computed point by point from positions during consecutive 10-s intervals. (*C*) Fourier analysis of velocity fluctuations derived from the velocity traces in *B*, illustrating cyclical fluctuations with a characteristic period of ≈2 min. (*D*) Distribution of instantaneous T cell velocities. Lateral (*x*–*y*) velocities were measured from point-to-point tracks at 10-s intervals (n = 2,930 measurements in three experiments). Velocities <3 μm·min^{-1} correspond to pauses of motile cells rather than to a population of nonmotile cells.

thelial venules (HEVs). We were able to verify intact microcirculation by the rapid motion of dim, unstained cells and occasional CFSE-labeled T cells. The fast acquisition rate (30 frames s^{-1}) of the 2P microscope allowed capture of sequential images of CFSE-labeled T cells as they streaked rapidly through the microcirculation (Fig. 2*B*).

Characterization of T Cell Locomotion *in Vivo*. To analyze the motility of T cells within the diffuse cortex of the node, we acquired 3D image stacks sequentially at 10-s intervals and tracked the *x*,*y* coordinates of individual T cells in a *z*-axis projection. As shown in Fig. 3*A*, T cells exhibited a stop-and-go pattern of motility, alternately lunging forward at relatively high velocity and then rounding up. The trailing edge often lagged far behind the cell, while the leading edge probed and moved forward. For individual cells, plots of instantaneous lateral velocity versus time revealed surges in velocity with peaks ≈25 μm·min^{-1} interspersed with phases of low motility (Fig. 3*B*). To look for periodicity in these velocity changes, we performed a Fourier analysis (Fig. 3*C*) on velocity traces from single cells. Typically, a single prominent peak emerged, indicating that T cell velocities fluctuated with periods of 1.6–2.4 min. In three experiments analyzed in detail, T cells displayed average velocities of 10.2–11.5 μm·min^{-1}, with peak velocities that exceeded 25 μm·min^{-1} (Fig. 3*D*). These results are similar to values we previously obtained for DO11.10 T cells in explanted lymph nodes (24), but contrast sharply with other results in explanted nodes by using confocal microscopy (30). Although the distribution of velocities (Fig. 3*D*) revealed a small percentage (5.8%) of cells moving <3 μm·min^{-1}, this predominantly reflected momentary pauses of individual cells rather than a population of nonmotile cells. WT BALB/c T cells displayed similar velocity distributions, with a higher and more variable percentage of nonmotile cells, e.g., Fig. 3*A*, presumably cells activating in response to endogenous antigens.

Analysis of Lateral T Cell Migration. In overlays of consecutive images, fluorescent T cells etched out tracks that criss-crossed the *x*–*y* landscape (data not shown) and did not reveal preferred trafficking paths over the time span of our records. To analyze the lateral migratory behavior of T cells (movement parallel to the capsule), we created an overlay of normalized T cell tracks from 39 individual cells (Fig. 4*A*). This plot revealed a symmetrical distribution of T cell trajectories, with no indication of bulk flow. Furthermore, in three separate image sequences, we plotted the normalized displacement of the mean population positions over time (Fig. 4*A Inset*). These mean positions varied only slightly around the starting point (<10 μm over 12 min) and showed no progressive displacement over time, as would be expected if collective migration occurred by chemotaxis in the T cell areas. Moreover, individual T cells showed displacements from a given starting point that increased proportionally with the square root of time over intervals longer than a few minutes (R^2 = 0.98), indicating that migration proceeds effectively as a random walk (Fig. 4*B*). In contrast, at shorter periods (<3 min) T cell displacements increased about linearly with time (velocity = 10.7 μm·min^{-1}), indicating that cells follow a "mean free path" of ≈30 μm along any given trajectory before a change in course becomes likely.

Although the above analysis provided no support for large-scale directed motion of T cells, it did not rule out the existence of localized (<20 μm) directional gradients that might be

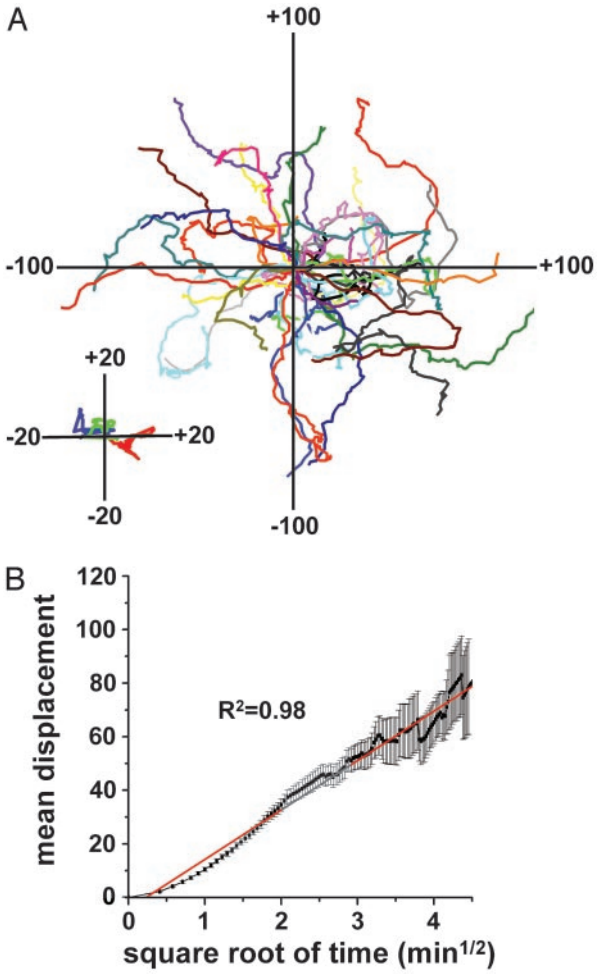

Fig. 4. T cell migration proceeds autonomously through the T cell areas. (*A*) Overlay of 39 individual T cell tracks plotted after aligning their starting positions. Cells were tracked over a 12-min period. (*Inset*) Shown are the mean coordinates of entire populations of T cells. Units are in μm. (*B*) Plot shows the mean absolute displacement of individual T cells ($n = 3$ experiments) away from their starting points as a function of square root of time. A random walk process is expected to yield a straight line on this transformed scale, and the red line shows a linear regression to the data. Error bars are ±SEM.

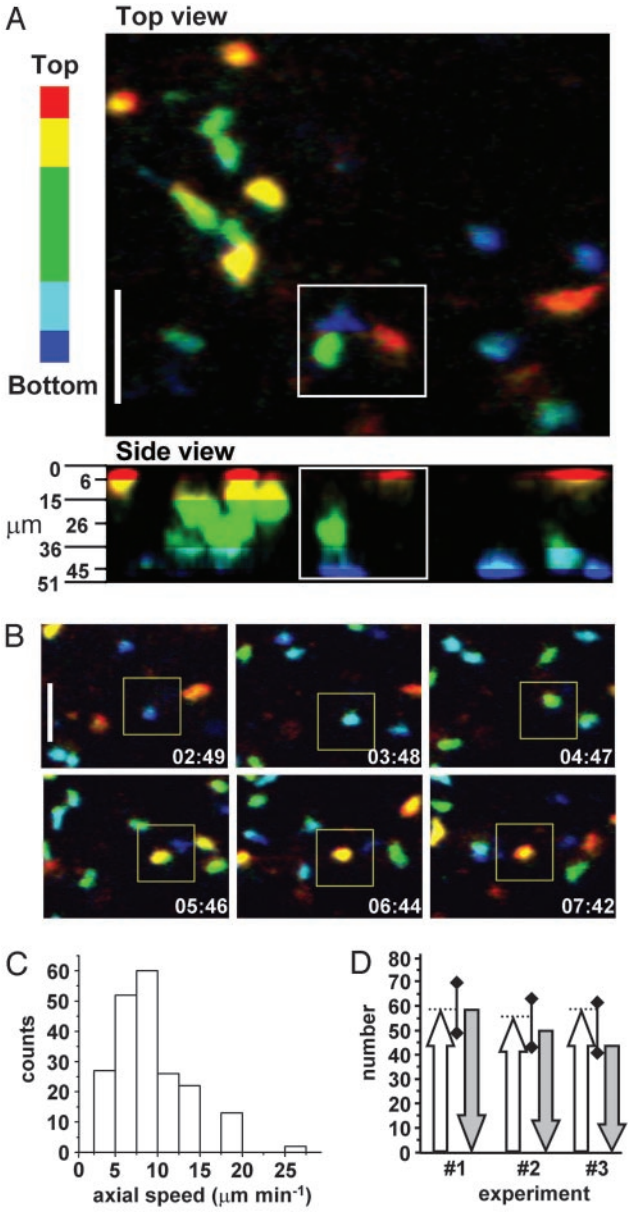

Fig. 5. Axial motion of T cells. (Scale bars, 25 μm.) (*A*) Color encoding of axial position of T cells. Representative images derived from a single *z*-stack, showing compressions along the *z* axis (top view) and *y* axis (side view). The axial (*z*) depth of cells within the stack is encoded by a pseudocolor scheme as illustrated in the side view [red, top 6 μm of stack (closer to the capsule); yellow, 6–15 μm; green, middle 30 μm; cyan, 36–45 μm; blue, 45–51 μm]. (*B*) Time-lapse image sequence, using color-encoding to allow tracking of T cells in 3D. Boxes frame a cell that began at the bottom of the imaging volume and moved upward toward the capsule. The complete image sequence can be viewed in Movie 1. (*C*) Distribution of T cell speed in the *z* axis (up or down). (*D*) Bar graph showing numbers of cells tracked as moving upward (toward the capsule) or downward. Data are from three experiments. Error bars indicate 95% confidence interval for a binomial distribution consistent with random cell trafficking in the *z* axis.

present at specialized sites, including those at which T cells enter the lymph node tissue from the circulation. Accordingly, we examined sites of homing for possible indications of preferential migration. We observed several instances in which rapidly moving T cells circulating in the blood suddenly adhered at particular locations, and then, after extravasation, began to migrate (Movie 1, which is published as supporting information on the PNAS web site, www.pnas.org). In such cases where cells directly entered the T cell zone from vessels at sites within 10 μm of each other, these newly resident T cells moved off in random directions, again taking autonomous paths within the node at the very start of their migration.

Analysis of Axial T Cell Migration. By virtue of the 2P optical section, our multidimensional data sets also contain *z*-axis information. However, the axial resolution is not as good as the lateral resolution, owing both to the elongated point-spread function of the microscope and to the relatively coarse (3 μm) *z*-axis step size. Tracking cell movement in the *z* axis is further complicated by difficulty in the display and analysis of 3D spatial information over time. To study axial T cell migration (movement perpendicular to the capsule), we therefore developed a color-encoding scheme to represent the axial position of cells in the imaging volume (see *Materials and Methods*). The axial speed of T cells was then calculated by measuring the time required for cells to traverse a 9-μm axial distance between two color boundaries. For example, the first two panels in Fig. 5*B* show a T cell (enclosed by box) that moved upward from the bottom of

the volume and crossed the 9-μm deep cyan region in $\approx$1 min (see Movie 1). A histogram of T cell speeds derived in this way (Fig. 5*C*) gave an average axial speed of 9.0 μm·min^{-1}, a value consistent with expectations based on our measurement of lateral velocity. The color-encoded records further allowed us to examine whether there was preferential migration of T cells axially toward or away from the overlying capsule. We looked at cells entering and leaving the imaging volume and scored them as either moving up (i.e., entering through the bottom plane or leaving the top) or down (entering through the top plane or leaving the bottom). Data from three experiments showed no significant difference in the proportion of cells moving either up or down as compared with chance (95% confidence interval for a binomial distribution; Fig. 5*D*). Thus, T cells appear equally likely to move toward or away from the capsule, similar to the random migration observed in the *x*–*y* plane.

Discussion

In secondary lymphoid organs, T cell motility is required for migration within the T cell zone and for making contacts with antigen-presenting dendritic cells. After activation, motility permits the escape of T cells from the lymph node and is essential for entrance into peripheral tissues to exert effector function (31). In this study, we combined intravital microscopy with 2P imaging to document the motility of naïve T cells in peripheral lymph nodes *in vivo*. T cell motility within the surgically exposed, but otherwise untouched, inguinal lymph node is sustained and vigorous. Except for momentary pauses, few cells are truly nonmotile. Instead, cells move with an average velocity of $\approx$11 μm·min^{-1} by a sequence of lunging motions, often achieving peak velocities $>$25 μm·min^{-1} before pausing, and then repeating this cycle with a periodicity of $\approx$2 min. T cells take a meandering course through the tissue and make occasional abrupt turns that distribute the cells randomly in all (*x*, *y*, *z*) dimensions. Our results define the default trafficking program of naïve T cells within the T cell areas in the absence of cognate antigen.

Two-photon microscopy was introduced over a decade ago (23), but has primarily found application in the fields of neurobiology and developmental biology (32, 33). In comparison with single-photon techniques (including confocal microscopy), 2P excitation has important advantages in that the longer wavelength light penetrates hundreds of μm into tissues and causes less photodamage, making it well suited to the study of lymphocytes *in vivo* (34). An important step toward studying T cell behavior *in vivo* was accomplished by recent experiments that imaged lymphocytes within explanted lymph nodes (24, 30) and spleen (25), providing a first glimpse of lymphocyte behavior in intact tissue. We previously showed that T cells are strikingly motile (average velocity of $\approx$12 μm·min^{-1}) when viewed with 2P microscopy in explanted nodes (24), consistent with findings reported here. However, with confocal imaging T cells were reportedly nonmotile in the absence of antigen, moving only after becoming activated (30). Because lymphatic and circulatory connections are disrupted in explanted preparations, conditions such as the level of tissue oxygenation may be unphysiological (30, 35, 36). Although the present study does not specifically address these issues, the robust motility seen with intravital imaging represents the physiological behavior of T cells *in vivo* and validates the use of explanted nodes to study T cell motility under appropriate conditions (24).

Naïve T cells possess an autonomous migratory program analogous to a random walk that allows them to cover a broad territory in a seemingly chaotic manner. During a typical motility cycle that lasts $\approx$2 min, T cells propel themselves forward several tens of micrometers along a given trajectory before pausing. The depth-encoded representation of cells within the imaging volume makes it clear that pauses are a genuine aspect of T cell behavior, rather than an artifact of continued motion purely in the *z* axis. Over a period of several minutes, the accumulation of turns gradually generates a 3D random walk; turn initiation may involve intracellular calcium, PKC, or integrin signaling pathways that have been shown to regulate motility and turning behavior of T cells *in vitro* (15, 16). The measured periodicity of the motility cycle *in vivo* is similar to that described for activated human CD4$^+$ T cells, HIV-induced syncytia, and a mouse T cell hybridoma on a variety of *in vitro* substrates (13, 14, 16), suggesting that an intrinsic control mechanism may be the basis for periodicity. However, it is important to emphasize that despite a common migratory program, T cells do not behave uniformly. For example, T cells clearly interact with elements in their environment such as reticular fibers and other cells (24). Furthermore, rapid motion perpendicular to the capsule was observed in specific regions that we have referred to as portals (24). In addition, our analysis was restricted to T cell zones, and further studies are needed to assess whether chemotactic migration exists in other regions, or under the influence of lymph-borne inflammatory signals (37).

A body of circumstantial evidence has suggested that chemokine gradients are the basis for the cellular compartmentalization of secondary lymphoid organs (38–41). However, it is unclear whether the chemokines function by forming chemotactic gradients or, alternatively, by regulating motility. In our experiments, T cells were observed to home directly into T cell areas (Movie 1), as opposed to entering this compartment by chemotaxis along gradients in the tissue parenchyma. The segregation of B and T cells across compartment-specific regions of the HEV has been observed in lymphocyte homing to Peyer's patches and lymph node (42). In conjunction with this regional homing mechanism, chemokines, extracellular matrix, and cell-to-cell contacts may function by forming a substrate for motility and could promote compartmentalization by creating physical boundaries or diffusion traps. This model is consistent with preliminary evidence that T cell motility is decreased near follicular boundaries (unpublished data) and the observation that newly resident T cells immediately migrate along random trajectories subsequent to homing.

Imaging approaches are precipitating a paradigm shift in our view of immune cells. Viewed with 2P microscopy, cells of the immune system behave as dynamic individuals and display a remarkable degree of motility and morphological complexity. T cells do not migrate collectively along pervasive chemokine gradients in the T cell zone, but move autonomously with each cell taking an independent trafficking path. The migration of T cells can be likened to that of solitary sharks on the hunt rather than a school of fish moving in concert. Antigen recognition may rely on a stochastic process in which chance encounters take place between highly motile T cells and antigen-bearing dendritic cells; such a mechanism would make it unnecessary to invoke T cell chemokine gradients as a requirement to orchestrate this interaction. We propose that T cell trafficking and antigen recognition may best be modeled as a multiagent system that displays decentralized intelligence, an algorithm originally identified in foraging ants and broadly applied in computer science and engineering (43). In these cases, each element or cell within the ensemble acts independently, yet collectively their behaviors satisfy a higher-order goal. In the case of the T cell, autonomous, random migration within the lymph node may be the optimal strategy to find the antigenic equivalent of a needle in the haystack.

We thank Arsalan Hejazi and Sabrina Duim-Quirk for assistance in image analysis and Luette Forest for care and breeding of the DO11.10 mouse strain. We also thank Jason Cyster and Taka Okada for valuable discussion. This research was supported by National Institutes of Health Grants GM-41514 (to M.D.C.) and GM-48071 (to I.P.).

1. Rowley, D. A., Gowans, J. L., Atkins, R. C., Ford, W. L. & Smith, M. E. (1972) *J. Exp. Med.* **136,** 499–513.
2. Sprent, J., Miller, J. F. & Mitchell, G. F. (1971) *Cell. Immunol.* **2,** 171–181.
3. Gowans, J. L. & Uhr, J. W. (1966) *J. Exp. Med.* **124,** 1017–1030.
4. Ford, W. L. & Atkins, R. C. (1971) *Nat. New Biol.* **234,** 178–180.
5. von Andrian, U. H. & Mackay, C. R. (2000) *N. Engl. J. Med.* **343,** 1020–1034.
6. Kaldjian, E. P., Gretz, J. E., Anderson, A. O., Shi, Y. & Shaw, S. (2001) *Int. Immunol.* **13,** 1243–1253.
7. Zlotnik, A. & Yoshie, O. (2000) *Immunity* **12,** 121–127.
8. Cyster, J. G. (1999) *Science* **286,** 2098–2102.
9. Cyster, J. G. (2000) *Curr. Biol.* **10,** R30–R33.
10. Mackay, C. R. (2001) *Nat. Immunol.* **2,** 95–101.
11. Moser, B. & Loetscher, P. (2001) *Nat. Immunol.* **2,** 123–128.
12. Gowans, J. L. (1996) *Immunol. Today* **17,** 288–291.
13. Shutt, D. C., Stapleton, J. T., Kennedy, R. C. & Soll, D. R. (1995) *Cell. Immunol.* **166,** 261–274.
14. Sylwester, A., Shutt, D., Wessels, D., Stapleton, J. T., Stites, J., Kennedy, R. C. & Soll, D. R. (1995) *J. Leukocyte Biol.* **57,** 643–650.
15. Dustin, M. L., Bromley, S. K., Kan, Z., Peterson, D. A. & Unanue, E. R. (1997) *Proc. Natl. Acad. Sci. USA* **94,** 3909–3913.
16. Negulescu, P. A., Krasieva, T. B., Khan, A., Kerschbaum, H. H. & Cahalan, M. D. (1996) *Immunity* **4,** 421–430.
17. Blaheta, R. A., Hailer, N. P., Brude, N., Wittig, B., Leckel, K., Oppermann, E., Bachmann, M., Harder, S., Cinatl, J., Scholz, M., *et al*. (2000) *Transplantation* **69,** 588–597.
18. Gunzer, M., Schafer, A., Borgmann, S., Grabbe, S., Zanker, K. S., Brocker, E. B., Kampgen, E. & Friedl, P. (2000) *Immunity* **13,** 323–332.
19. Friedl, P. & Gunzer, M. (2001) *Trends Immunol.* **22,** 187–191.
20. Dustin, M. L., Allen, P. M. & Shaw, A. S. (2001) *Trends Immunol.* **22,** 192–194.
21. von Andrian, U. H. (1996) *Microcirculation* **3,** 287–300.
22. Okada, T., Ngo, V. N., Ekland, E. H., Forster, R., Lipp, M., Littman, D. R. & Cyster, J. G. (2002) *J. Exp. Med.* **196,** 65–75.
23. Denk, W., Strickler, J. H. & Webb, W. W. (1990) *Science* **248,** 73–76.
24. Miller, M. J., Wei, S. H., Parker, I. & Cahalan, M. D. (2002) *Science* **296,** 1869–1873.
25. Wei, S. H., Miller, M. J., Cahalan, M. D. & Parker, I. (2002) *Adv. Exp. Med. Biol*. **512,** 203–208.
26. Bousso, P., Bhakta, N. R., Lewis, R. S. & Robey, E. (2002) *Science* **296,** 1876–1880.
27. Papaioannou, V. E. & Fox, J. G. (1993) *Lab. Anim. Sci.* **43,** 189–192.
28. Thompson, J. S., Brown, S. A., Khurdayan, V., Zeynalzadedan, A., Sullivan, P. G. & Scheff, S. W. (2002) *Comp. Med.* **52,** 63–67.
29. Nguyen, Q. T., Callamaras, N., Hsieh, C. & Parker, I. (2001) *Cell Calcium* **30,** 383–393.
30. Stoll, S., Delon, J., Brotz, T. M. & Germain, R. N. (2002) *Science* **296,** 1873–1876.
31. Campbell, J. J., Haraldsen, G., Pan, J., Rottman, J., Qin, S., Ponath, P., Andrew, D. P., Warnke, R., Ruffing, N., Kassam, N., *et al*. (1999) *Nature* **400,** 776–780.
32. Yuste, R. & Denk, W. (1995) *Nature* **375,** 682–684.
33. Squirrell, J. M., Wokosin, D. L., White, J. G. & Bavister, B. D. (1999) *Nat. Biotechnol.* **17,** 763–767.
34. Cahalan, M. D., Parker, I., Wei, S. H. & Miller, M. J. (2002) *Nat. Rev. Immunol.* **2,** 872–880.
35. von Andrian, U. H. (2002) *Science* **296,** 1815–1817.
36. Caldwell, C. C., Kojima, H., Lukashev, D., Armstrong, J., Farber, M., Apasov, S. G. & Sitkovsky, M. V. (2001) *J. Immunol.* **167,** 6140–6149.
37. Gretz, J. E., Norbury, C. C., Anderson, A. O., Proudfoot, A. E. & Shaw, S. (2000) *J. Exp. Med.* **192,** 1425–1440.
38. Legler, D. F., Loetscher, M., Roos, R. S., Clark-Lewis, I., Baggiolini, M. & Moser, B. (1998) *J. Exp. Med.* **187,** 655–660.
39. Nakano, H., Mori, S., Yonekawa, H., Nariuchi, H., Matsuzawa, A. & Kakiuchi, T. (1998) *Blood* **91,** 2886–2895.
40. Forster, R., Schubel, A., Breitfeld, D., Kremmer, E., Renner-Muller, I., Wolf, E. & Lipp, M. (1999) *Cell* **99,** 23–33.
41. Gunn, M. D., Kyuwa, S., Tam, C., Kakiuchi, T., Matsuzawa, A., Williams, L. T. & Nakano, H. (1999) *J. Exp. Med.* **189,** 451–460.
42. Warnock, R. A., Campbell, J. J., Dorf, M. E., Matsuzawa, A., McEvoy, L. M. & Butcher, E. C. (2000) *J. Exp. Med.* **191,** 77–88.
43. Bonabeau, E., Dorigo, M. & Theraulaz, G. (2000) *Nature* **406,** 39–42.